



# Prediction of reinforced concrete walls shear strength based on soft computing-based techniques

Alireza Tabrizikahou<sup>1</sup> · Gordana Pavić<sup>2</sup> · Younes Shahsavani<sup>3</sup> · Marijana Hadzima-Nyarko<sup>2</sup>

Accepted: 10 July 2023 / Published online: 20 July 2023  
© The Author(s) 2023

## Abstract

The precise estimation of the shear strength of reinforced concrete walls is critical for structural engineers. This projection, nevertheless, is exceedingly complicated because of the varied structural geometries, plethora of load cases, and highly nonlinear relationships between the design requirements and the shear strength. Recent related design code regulations mostly depend on experimental formulations, which have a variety of constraints and establish low prediction accuracy. Hence, different soft computing techniques are used in this study to evaluate the shear capacity of reinforced concrete walls. In particular, developed models for estimating the shear capacity of concrete walls have been investigated, based on experimental test data accessible in the relevant literature. Adaptive neuro-fuzzy inference system, the integrated genetic algorithms, and the integrated particle swarm optimization methods were used to optimize the fuzzy model's membership function range and the results were compared to the outcomes of random forests (RF) model. To determine the accuracy of the models, the results were assessed using several indices. Outliers in the anticipated data were identified and replaced with appropriate values to ensure prediction accuracy. The comparison of the resulting findings with the relevant experimental data demonstrates the potential of hybrid models to determine the shear capacity of reinforced concrete walls reliably and effectively. The findings revealed that the RF model with RMSE = 151.89, MAE = 111.52, and  $R^2 = 0.9351$  has the best prediction accuracy. Integrated GAFIS and PSOFIS performed virtually identically and had fewer errors than ANFIS. The sensitivity analysis shows that the thickness of the wall ( $b_w$ ) and concrete compressive strength ( $f_c$ ) have the most and the least effects on shear strength, respectively.

**Keywords** Soft computing techniques · ANFIS · RF · PSO · Reinforced concrete wall · Shear strength

## List of symbols

$\lambda$	Modification factor to represent lightweight concrete's mechanical properties characteristics when compared to standard weight concrete with the same compressive strength	$\lambda$	Aspect ratio coefficient
$f_c$	Compressive strength of the cylinder concrete	$\rho_x$	Ratio of reinforcement by longitudinal reinforcement
$\alpha_c$	Aspect ratio coefficient	$\rho_y$	Transverse reinforcement ratio
$\alpha$	Inclination between compressive load and wall alignment	$\sigma_{cp}$	Axial compress stress
		$A_{cv}$	Effective cross-sectional area of the concrete
		$A_g$	Gross area of the wall
		$A_{sw}$	Cross-sectional area of shear reinforcement within s
		$b_w$	Thickness of the wall
		$C_{Rd,c}$	$0.18 \gamma_c$ ( $\gamma_c$ equals to 0.15)
		d	Effective depth of the cross section
		$f_{ck}$	Characteristic compressive cylinder strength of concrete at 28 days
		$f_c$	Concrete compressive strength ( $f_c \approx 0.838 f'_c$ )
		$F_{yt}$	Strength of horizontal bars
		$F_{yv}$	Yield strength of bars at vertical direction of wall
		$f_{ywd}$	Yield strength of shear reinforcement
		$h_w/l_w$	Height-to-length ratio
		$h_w$	Height of the wall

✉ Alireza Tabrizikahou  
alireza.tabrizikahou@doctorate.put.poznan.pl

<sup>1</sup> Institute of Building Engineering, Poznan University of Technology, Piotrowo 5, 60-965 Poznan, Poland

<sup>2</sup> Faculty of Civil Engineering and Architecture Osijek, Josip Juraj Strossmayer University of Osijek, Vladimira Preloga, 31000 Osijek, Croatia

<sup>3</sup> Faculty of Engineering, Kharazmi University, Tehran 15719-14911, Iran

$k_1$	A variable of 0.15 that accounts for the impact of $N_u$ on the stress pattern
$L_w$	Length of the wall
$M_u$	Moment at the section
$N_u$	Axial load
$s$	Spacing of the horizontal reinforcement bar
$V_{exp}$	Experimentally shear strength
$V_n$	Predicted the shear strength
$V_u$	Maximum shear force
$z$	Lever of internal forces ( $\approx 0.9d$ )

**Table 1** Algorithm used in modelling the compressive strength of rubberized concrete and shear concrete wall

Algorithm	Data points	References
PSO	209	Baghi and Siavashi (2019)
ANN	369	Nguyen et al. (2021)
RF-based	393	Mangalathu et al. (2020)
GP	254	Gondia et al. (2020)
ANN-AHS, -HS, -GHS	500	Keshtegar et al. (2021)
SVR-RSM	500	Keshtegar et al. (2021)

## 1 Introduction

Reinforced concrete walls (RCW) are widely employed in structures that are subjected to significant lateral loadings, such as wind and earthquake loads (Hadzima-Nyarko 2015) (Nikoo et al. 2017). RCWs frequently function as cantilever beams with a rigid base, bearing loads down to the foundations (Darwin et al. 2016) (Al-Furjan et al. 2022). These structural elements are susceptible to fluctuating shear, which normally achieves its greatest value at the bottom, bending moments with tensile stress located near the loaded tip and compressive stress towards the distant extremity, and vertical compression owing to gravity loads. RCWs with a low height-to-length proportion are mostly governed by shear load, whereas those with a high height are primarily influenced by bending design specifications.

The design principle of RCW is typically identical to that of beams. These conventional approaches depend heavily on imprecise inductive calculations, which have several drawbacks. The ACI318 design code (Committee 1995), for example, excludes the influence of longitudinal shear reinforcement, whereas the Eurocode (Code 2005) implies that the shear capacity of RCW with a height-to-length proportion of 2 or more is exclusively dependent on transverse shear reinforcement. RCW must be constructed to be malleable in nature. As a result, its mechanical integrity should be determined by flexure rather than shear. As a result, precise modelling of the shear strength of RCW is critical (Asgharpoor et al. 2021) (Keshtegar et al. 2022) (Tabrizikahou et al. 2022).

Nonetheless, given the plethora of structural implementations and load combos that may occur on an RCW, comprehensive knowledge of its structural behaviour is indeed very complicated (Teng and Chandra 2016) (Piri et al. 2023). For example, low-rise RCW may have a height-to-length ratio of less than 2, but taller structures may have a proportion significantly more than 2 Chandra et al. (2018), (Zhu et al. 2022). RCW may also have a variety of geometrical layouts, reinforcing schemes, and gravitational and seismic loads. Given the complexities of RCW, many laboratory investiga-

tions have been undertaken to fully understand its structural behaviour (Al-Furjan et al. 2022) (Al-Furjan et al. 2022).

One of the fundamental phases in the design of structural components of reinforced concrete (RC) structures is the assessment of shear capability. Up to now, many academics and structural design codes have suggested multiple mechanical approaches to analyse the shear strength of RCW (Hadzima-Nyarko et al. 2021) (Kolahchi et al. 2022) (Tabrizikahou et al. 2022). A simple solution to the problem involves the structural code or a scientific investigation that considers numerous factors; nevertheless, both techniques provide significantly varied shear strength findings (Armaghani et al. 2019) (Marzok et al. 2020) (Luo et al. 2022). The absence of appropriate and dependable experimental or theoretical relationships for evaluating the shear capacity of RCWs has caused in the last two decades to pique the attention of academics working with non-deterministic approaches.

Various researchers used different methods to model the shear strength of RCWs. Some of the studies are summarized in Table 1.

The findings of the preceding investigations are undoubtedly promising, particularly given the applications of soft computing models to predict the shear strength of RCWs is still in their early stages. As a result, this study investigates the use of fuzzy-based techniques (GAFIS, PSOFIS, and ANFIS) for estimating the shear strength of RCWs. For network training, a research database is employed that is accessible in the literature and is concerned with the shear resistance of RCWs specimens of varied sizes, materials, and geometric characteristics. Since RF is a powerful prediction approach that has not been studied in forecasting the shear strength of RCWs, it is beneficial to compare its capabilities with GAFIS, PSOFIS, and ANFIS to see which way is best.

The purpose of this research is to create the RF technique as a reliable and efficient machine-learning model for predicting the shear strength of RCWs. The application of the RF model in the prediction of the shear strength of RCWs might help catch patterns in huge numbers of data obtained from empirical studies. The results of the created RF are thoroughly compared with three other robust artificial intel-

ligence techniques, namely ANFIS, GAFIS, and PSOFIS. To the authors’ knowledge, this is the very first time the RF technique has been used to determine the shear strength of RCWs.

This paper’s novelty stems from its revolutionary way of evaluating the shear strength of reinforced concrete walls using soft computing-based methodologies. Traditional methods for constructing these structures usually rely on empirical formulations, which have limitations and produce low forecast precision. This work, on the other hand, overcomes these difficulties by utilizing the capabilities of soft computing models.

To increase shear capacity estimation reliability, the fuzzy model’s membership function range is improved by utilizing ANFIS, GA, and PSO techniques. Furthermore, the results of the developed models are compared to those of the RF model, revealing a novel use of RF in forecasting the shear strength of reinforced concrete walls.

The research also contributes to resolving the limitations of standard empirical approaches by providing an analysis of the key parameters of shear strength and investigating the use of soft computing models. The findings highlight the significance of components such as wall thickness and concrete compressive strength, supplying significant information to engineers and designers.

Section 2 presents and explains the main parameters which influence the shear strength of RCWs. Section 3 provides a comprehensive analysis of the state-of-the-art in modelling RCWs. Section 4 introduces the hybrid and RF methodologies, including the formulas and modelling layers, as well as the numerous statistical measures used to compare the different models. Section 5 then describes the characteristics of the innovative modelling techniques used in this work. Section 6 delves deeply into the model outputs, taking into account reliability, propensity, and variability. Section 7 discusses and compares the outcomes achieved by various methodologies. Finally, Sect. 8 illustrates the implications that may be taken from this research.

## 2 Influencing parameters

Physical, experimental, numerical, and statistical models are used to determine the lateral load-bearing capacity of RCWs in many building codes, specifications, and regulations. Most of these design regulations give a variety of layouts and statistical approaches for determining the shear capacity of RCWs. In these design codes, the shear strength of the RCWs is generally ascribed to the concrete ( $V_c$ ) and reinforcement ( $V_s$ ) shear strength and is determined using Eq. 1.

$$V_u = V_c + V_s \tag{1}$$

However, to define the concrete and reinforcement shear strength, there are various ideas. ACI318-14-11 (American Concrete Institute 2014) proposed Eqs. 2 and 3 to calculate the values of ( $V_s$ ) and ( $V_c$ ).

$$V_s = \frac{A_v f_{yt} d}{s} \tag{2}$$

$$V_c = \min \left\{ \left[ \left( 0.274 \lambda \sqrt{f_c} + \frac{N_u}{4l_w d} \right) h d \right] \left[ 0.05 \lambda \sqrt{f_c} + \frac{\left( 0.104 \lambda \sqrt{f_c} + 0.2 \frac{N_u}{l_w h} \right)}{\frac{M_u}{V_u l_w} - \frac{1}{2}} \right] h d \right\} \tag{3}$$

Additionally, based on ACI318-14-18 (American Concrete Institute 2014) the values of ( $V_s$ ) and ( $V_c$ ) can be defined by using Eqs. 4 and 5.

$$V_s = A_{cw} \times \rho_t f_{yt} \tag{4}$$

$$V_c = A_{cv} \times \alpha_c \lambda \sqrt{f_c} \tag{5}$$

Eurocode 8 (Code 2005) introduces Eqs. 6 and 7 to calculate the concrete and reinforcement shear strength.

$$V_s = \frac{A_{sw}}{s} z f_{ywd} \cot \alpha \tag{6}$$

$$V_c = \left[ C_{Rd,c} k (100 \rho_1 f_{ck})^{\frac{1}{3}} + k_1 \sigma_{cp} \right] b_w d \geq \left( 0.035 k^{\frac{2}{3}} f_{ck}^{\frac{1}{2}} + k_1 \sigma_{cp} \right) b_w d \tag{7}$$

Figure 1 illustrates the schematic of the concrete wall and the influencing parameters on the shear capacity of RCW such as concrete’s compressive strength, dimension proportion, applied load, transverse and longitudinal reinforcement proportions, and the wall’s gross area.

According to the formulae provided, the shear strength of RCWs is determined by the concrete’s compressive strength, applied load, azimuth and elevation reinforcement proportions, the wall’s cross-sectional area, the ratio of horizontal and vertical reinforcement and yield strength of the reinforcements. However, investigations by Wood (1990) and, Gulec et al. (2007) found that the lateral load-carrying capacity of RCWs results based on these empirical-based equations can be varied significantly based on different specifications. Therefore, in this study, different feasible methods are used to predict the shear capacity of RCWs.

## 3 Review of RCW modelling

Chandra et al. (2018) based on 84 different concrete walls developed a model for estimating the shear capacity of RCSW. Their results demonstrated that the model predicted the shear strength with about 0.36 difference ( $V_{exp}/V_n =$



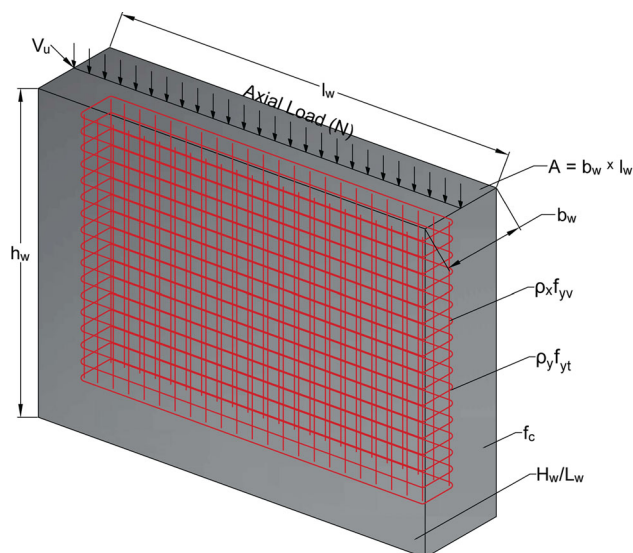


**Fig. 1** Schematic of the concrete wall and the influencing parameters studied in this paper

1.36) with a coefficient of variation (CoV) of 0.20. The suggested technique can also estimate the shear strength of RC walls with high accuracy over a wide variety of wall height-to-length ratios, concrete compressive strengths, and reinforcing percentages in the boundary components.

Baghi and Siavashi (2019) introduced a particle swarm optimization method for developing a quantitative formula for estimating the shear strength of RCSW that attributed to variations in the flexural stress criterion and the propensity of the essential perpendicular fracture, the impact of vertical and horizontal reinforcement capacity, the boundary column reinforcement throughout the length, and the dowel action. The model made use of a dataset that comprises 209 experimental data from the literature. The suggested model produced an average value of 1.13 with a COV of 33% by assessing the ratio between the experimental findings and the analytical predictions ( $V_{exp}/V_n$ ). The average values of  $V_{exp}/V_n$  for the models related to ACI318-14 and Chandra et al. were 1.08 and 1.17, respectively, with COVs of 52.0 and 47.0%.

Kusunoki et al. (2019) investigated pushover analysis, which is frequently used to assess failure modes and stress distribution at the risk ultimate limit. To validate the accuracy of these functions, they evaluated a large empirical record of 507 RCW trials. The anticipated initial stiffness was discovered to be underestimated, the final flexural and shear strengths were typically lower than the equivalent actual numbers, and reliability was dependent on the existence of boundary columns and the presence of apertures. Likewise, the anticipated yield and maximum shear strength deformations appeared to be lower than the empirical values. These

findings underscore the necessity for more precise and powerful prediction techniques.

Nguyen et al. (2021) scrutinized a machine-learning-based method for estimating the shear resistance of squat grooved RCW. They contended that available experimental models in current design codes and documented research result in considerable discrepancies in estimating shear capacity. As a consequence, they presented an ANN-based on 369 tests and 13 input factors gathered from the literature to more appropriately estimate the shear strength of squat flanged RCW than current algorithms. Furthermore, a prediction technique relying on the ANN framework was suggested to estimate the shear capacity of squat flanged walls, and a graphical interface system was developed to aid in functional design.

Mangalathu et al. (2020) researched the inadequate safety profitability of RCSW as well as the inadequacy of experimental models for instant failure mode assessment of current shear walls. They developed an appropriate statistical method using eight machine-learning methods based on a database of 393 empirical findings for shear walls with varied geometric arrangements. The random forest technique was devised and shown to be 86% accurate in determining the failure mechanism of shear walls. The important characteristics determining the failure mode of shear walls were discovered to be the wall aspect ratio, boundary element reinforcement coefficients, and wall length-to-wall thickness proportion.

Gondia et al. (2020) compared RCSW's squat with boundary functions to empirical data from several situations, accounting for the purported inaccuracy of relevant current shear strength prediction expressions like ASCE/SEI 43-05. By employing a dataset of 254 shear walls, genetic programming (GP) is used to suggest an expression of shear strength prediction. The RCSW's squat with fronting components, including suggested inexactness in critical current shear resistance forecasting terms such as ASCE/SEI 43-05, was evaluated using practical data from various circumstances.

Keshtegar et al. (2021) presented a hybrid machine intelligence system based on an ANN and an adaptive harmony search optimization (AHS) method for estimating the final shear strength of RCWs. Various quantitative measures were utilized to evaluate the effectiveness of the ANN model integrated with AHS (ANN-AHS) to three known experimental correlations and two ANN models linked with harmony search (ANN-HS) and global-best harmony search (ANN-GHS). Their findings showed that the suggested ANN-AHS model outperformed the ANN-HS and ANN-GHS models in estimating the shear strength of RCW and was more precise than the recognized experimental equations.

Keshtegar et al. (2021) examined a hybrid model to estimate the shear capacity of RCSW. The proposed modelling technique (RSM-SVR) is comprised of the integration of the

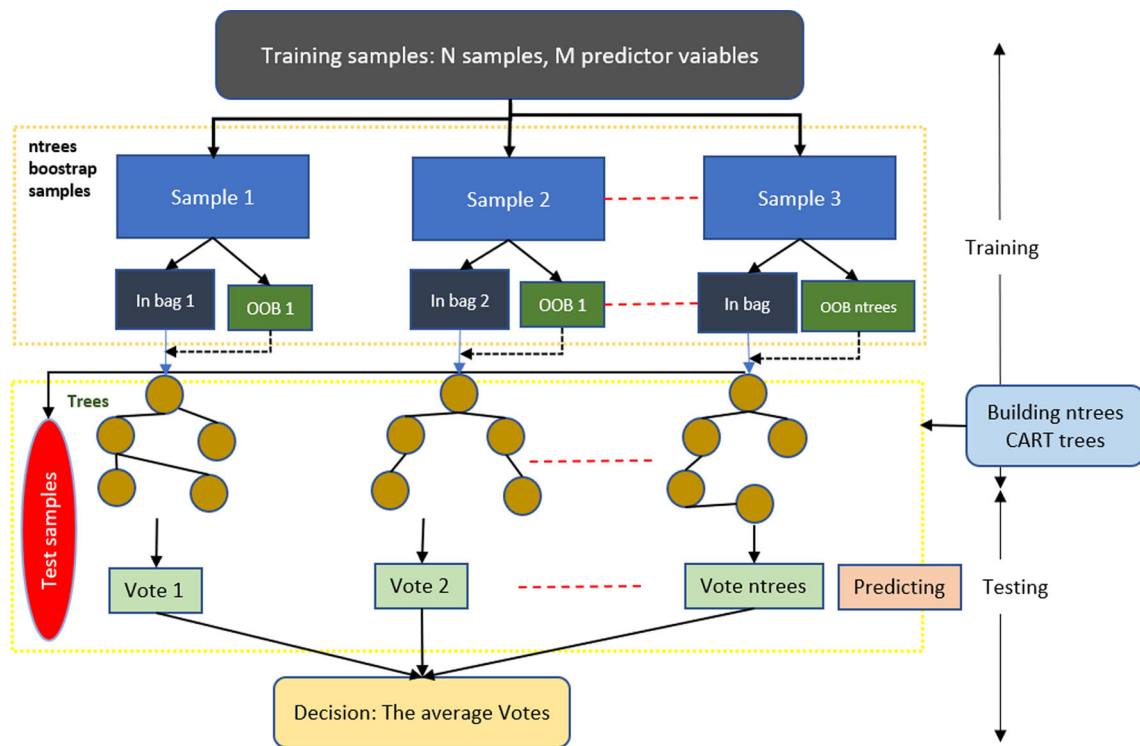


Fig. 2 Steps in the RF method

support vector regression (SVR) and response surface model (RSM) techniques. It was demonstrated that the suggested RSM-SVR modelling technique produced more precise estimates of RCSW shear strength. The method accurately appreciated the effect of the main design factors, exhibiting a consistent trend and significantly decreased ambiguity. As a result, the suggested model might be used in intelligent creative models and to improve relevant requirements in design codes.

## 4 Methodology

### 4.1 Random Forests (RF)

Breiman’s RF model was proposed as a powerful learning algorithm utilizing an assembly of decision trees (Breiman 2001). The RF is applied for both regression and classification issues. In the RF algorithm, each tree is grown on a separate training set that is a bootstrap replicate of the original data (Goudarzi and Shahsavani 2012). The suggested technique is built with a mix of decision trees created from arbitrary bootstrap samples of the input datasets. In comparison with a single regression tree, RF can reduce the risk of overfitting while improving prediction performance. The number of trees ( $n_{tree}$ ) and the predictor parameters ( $m_{try}$ )

are two essential factors for executing the RF method that may be used to modify the model. The following are the major processes for creating an RF model, as seen in Fig. 2:

- (1) Considering ( $n_{tree}$ ) in the forest.
- (2) Attributing to each tree a bootstrap sample of size  $n_{tree}$  from the input or training dataset.
- (3) Choosing a predictor ( $m_{try}$ ) from a training dataset with  $p$  randomly selected predictors for each node’s split point.
- (4) Distinguishing the split point and the best parameter from among predictors and dividing each node into two sub-nodes.
- (5) Anticipate the new data, i.e. the predictions, by summing the random forest since it is a strong model that can cope with a high-dimensional database with numerous predictors.

To minimize overfitting in random forest prediction, the major tuning parameters ( $n_{tree}$ ;  $m_{try}$ ) should be chosen carefully. The grid-search approach was used to optimize the RF values for the parameters  $n_{tree}$  and  $m_{try}$  at the same time, based on the root mean squared error (RMSE) of the out-of-bag (OOB) data for each parameter setting.

In this research, the values of  $n_{tree}=40$  and  $m_{try}=7$  was used to construct the final model.

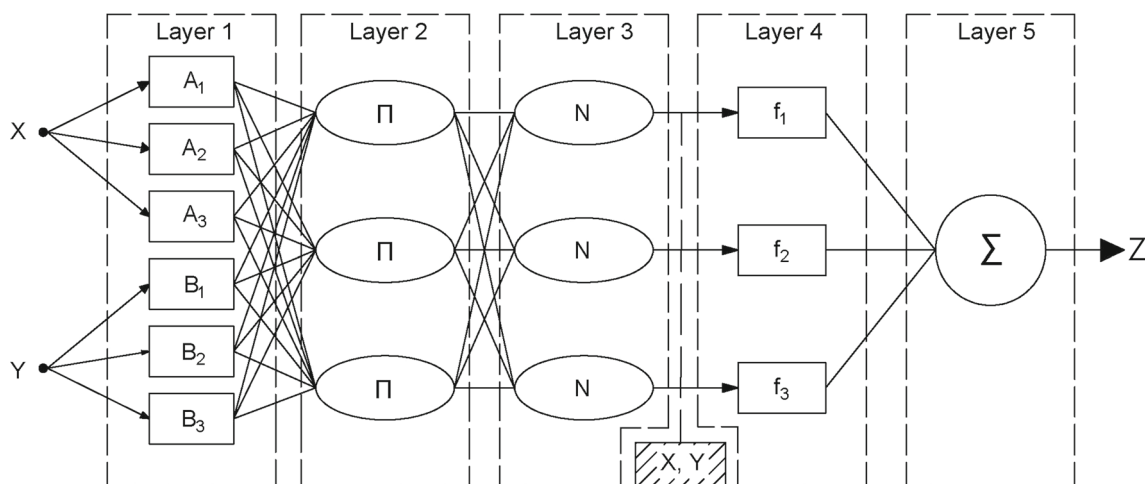


Fig. 3 A simple structure of ANFIS with two inputs

## 4.2 Fuzzy inference system (FIS)

To compare the results of ANFIS, PSOFIS, and GAFIS algorithms based on fuzzy rules, it is necessary to develop a fuzzy inference system. Fuzzification, fuzzy database, and defuzzification are the main sections of FIS. To build the Sugeno FIS structure, grid partitioning (GP) and subtractive clustering (SC) are used. Since the grid partitioning needs more computational effort compared to the subtractive clustering (Ansari et al. 2020), in this research genfis3 generates a FIS using fuzzy clustering by extracting a set of rules that models the data behaviour used. The number of clusters is equal to 5 with 100 iterations used for FIS development. The fuzzy rules in the Takagi and Sugeno fuzzy inference system (Takagi and Sugeno 1985) were used and are shown as follows:

$$f_i = p_i x + q_i y + r_i, \quad x = A_i, \quad y = B_i, \quad i = 1, 2, 3, \dots, n \quad (8)$$

## 4.3 Adaptive neuro-fuzzy inference system (ANFIS)

ANFIS is a multilayer network fuzzy inference system that provides a connectivity structure of Jang's Sugeno fuzzy system (Jang 1993). ANFIS functions in an equivalent way as artificial neural networks (ANN) and fuzzy inference systems (FIS).

To optimize the membership functions parameter, the approach employs a mix of back-propagation and least square (hybrid) or back-propagation (Chen 2013). Figure 3 depicts the ANFIS's overall design, which includes two inputs and one output. The ANFIS algorithm has five computation levels. Each layer's job is briefly discussed below.

Layer 1: Assigns a linguistic value to each input, such as small, medium, big, and so on. Every node is a node function

that adapts to its surroundings.

$$O_i^1 = \mu_{A_i}(X) \quad i = 1, 2, 3, \quad O_i^1 = \mu_{B_{i-3}}(Y) \quad i = 4, 5, 6 \quad (9)$$

The linguistic value with their member functions ( $\mu_{A_i}$  and  $\mu_{B_{i-3}}$ ) is the output of the first layer where X and Y are the node  $i$  model inputs,  $A_i$  and  $A_{i-3}$  are the linguist value.

Layer 2: Amplifies the input nodes. The outcome of this layer reflects firing strength, which indicates how well the norms match the inputs.

$$O_k^2 = w_k = \mu_{A_i}(X) \times \mu_{B_{i-3}}(Y), \quad i = 1, 2, \dots, 6, \quad k = 1, 2, 3 \quad (10)$$

where  $O_k^2$  or  $w_k$  is the firing strength of node  $k$ .

Layer 3: Determines each node's normalized firing strength. This strength's ratio of the  $k_{th}$  regulates to the sum of the firing strength principles.

$$O_k^3 = \bar{w}_k = \frac{w_k}{\sum w_k} = 1, 2, 3 \quad (11)$$

where  $O_k^3$  is the normalized firing strength of node  $k$ .

Layer 4: Determines the node function of each node as well as the effect of each node on the overall outcome.

$$O_k^4 = \bar{w}_k f_k = \bar{w}_k (p_k X + q_k Y + r_k) = 1, 2, 3 \quad (12)$$

Layer 5: Denotes the total output as a sum of all input nodes.

$$O_k^5 = Z = \sum \bar{w}_k f_k \quad k = 1, 2, 3 \quad (13)$$

The Gaussian membership function is utilized for model creation in this study, and the hybrid optimization approach

**Table 2** Summary of ANFIS model

Parameter	Value
Train epoch	100
Train-Error goal	0
Train-Initial step size	0.01
Train-Step size decrease	0.9
Train-Step size increase	1.1

**Table 3** Summary of GA parameters

Parameter	Value
Crossover ratio	0.7
Mutation ratio	0.5
Mutation rate	0.01
Selective pressure	8
Population	100
Maximum iteration	400

is applied for membership function (MF) parameters. The results of parameters used in the ANFIS model are summarized in Table 2.

#### 4.4 Integrated genetic algorithms with FIS (GAFIS)

Holland et al. (1992) established the search genetic algorithm (GA), which is a probabilistic and population-based optimization approach. Natural processes including heredity, mutation, crossover, and natural selection influenced the model’s concept (Rani and Moreira 2010) (Al-Obaidi et al. 2017) (Koza 1994). In each iteration, the optimizer strives for the best possible results by analysing and choosing the parent population from the triggered population using the roulette wheel method and the implementation of evolutionary operators, such as mutation and crossover, on the parent to generate the next generation.

The method begins by creating the starting population at random. The fitness function is then used to measure the individual’s fitness. Then, during the selecting step, techniques such as the Roulette Wheel are used (Goldberg 2006). The fitness of each population is determined using Eq. 14 in this technique.

$$p_i = \frac{f_i}{\sum_{i=1}^n f_i} \tag{14}$$

where  $p_i$  is the probability of individual,  $f_i$  is the fitness of individual, and  $n$  is the population size.

Crossover and mutation are two processors employed to produce offspring (Sharafati et al. 2020).

Table 3 provides an overview of the GA parameters that were employed in this study.

**Table 4** Summary of PSO parameters

Parameter	Value
Inertia weight ( $w$ )	1
Particle acceleration coefficient ( $c_1$ )	1
Global acceleration coefficient ( $c_2$ )	2
Population	35
Maximum iteration	800
Minimum value of particle	−100
Maximum value of particle	100

#### 4.5 Integrated particle swarm optimization with FIS (PSOFIS)

Particle swarm optimization (PSO) is a bio-inspired population-based algorithm that generates and uses random variables driven by the intelligent behaviour of wildlife swarms like birds or fish (Kennedy and Eberhart 1995).

First, the algorithm distributes the particles randomly within a given space of solutions. Then, the positions of the particles are assessed as the global best locations following their own experience as well as of the neighbours. Particles’ speed is computed since each particle has its velocity, and it does its own repeated selection for the optimum location. Eqs. 15 and 16 calculate velocity and new locations.

$$V_{i,(t+1)} = wV_{i,(t)} + c_1r_1(Bp_{i,(t)} - X_{i,(t)}) + c_2r_2(Bg_t - X_{i,(t)}) \tag{15}$$

$$X_{i,(t+1)} = X_{i,(t)} + V_{i,(t+1)} \tag{16}$$

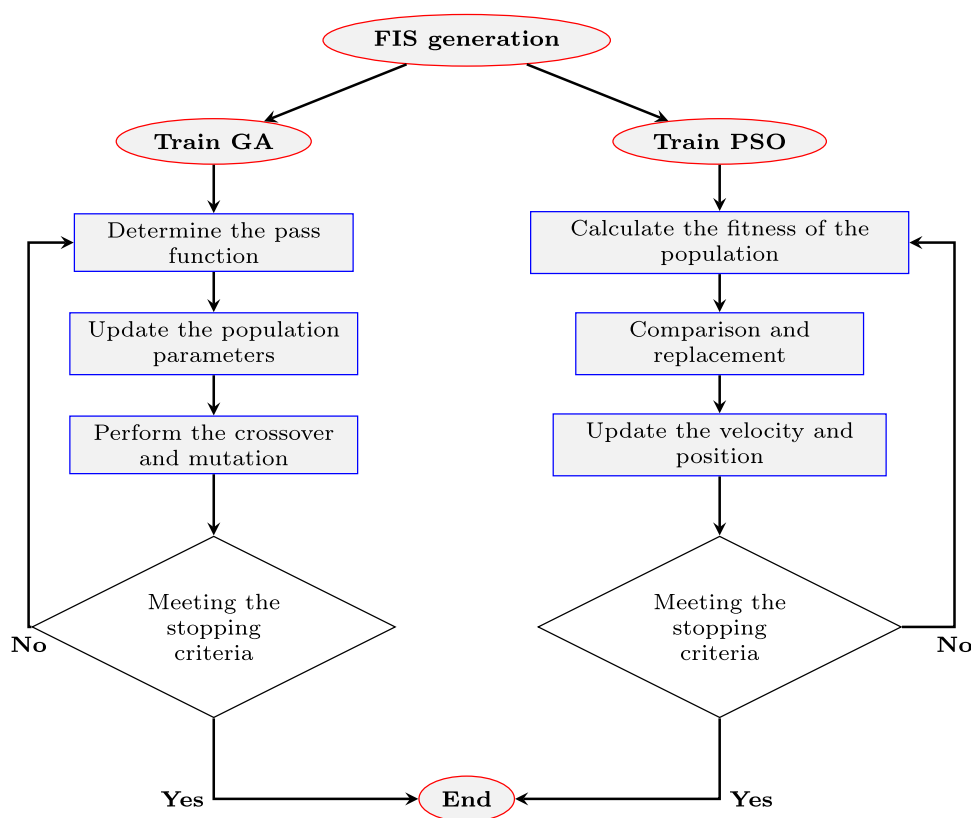
where  $w$  is inertial weight representing the impact of the velocity vector ( $V_i$ ) on the new vector,  $t$  is the velocity of particle  $i$  at iteration  $t$ ,  $c_1$  and  $c_2$  are acceleration constants,  $Bp_{i,(t)}$  and  $Bg_t$  are particle  $i$  and global best positions, respectively, and  $X_i, t$  is the present position of particle  $i$ .

The optimum location is referred to as the result or forecast of the outcome parameter. Locating a newer location is influenced by two criteria throughout the finding phase of every single unit; the first is the particle’s best experience up to that iteration. The steps are repeated as long as the stopping criteria are fulfilled.

PSO and GA algorithm was used in this study to optimize the parameters of the fuzzy inference system. In contrast to the GA method, the PSO algorithm may function effectively with a tiny population. The best local and global outcomes were identified by RMSE for each iteration. Table 4 lists all of the PSO parameters used in this study.

Figure 4 depicts the approaches utilizing GA and PSO.

**Fig. 4** Steps in PSO and GA model



## 5 Dataset for modelling process

The total number of data used in this dataset comprised of 143 experimentally tested RCWs. The dataset was divided into train and test data sets at random. 65% (95 number) of the data was chosen for model creation, while the remaining 48 numbers (35%) was chosen to test the performance of the generated model. As a result, the model's liability is assessed on data that is unknown to the model and was not provided during the training stage.

Table 5 shows the statistical characteristics of the input variables and the related maximum force ( $V_u$ ) for the datasets.  $X_{\min}$ ,  $X_{\max}$ , mean, and standard deviation (STD) are the variables' minimum, maximum, average, and standard deviation, respectively.

$L_w$ ,  $h_w$ , and  $b_w$  represent length, height, and thickness of the wall, respectively.  $A_g$  is the gross area of the wall,  $h_w/l_w$  is height-to-length ratio,  $\rho_x$  is ratio of reinforcement by longitudinal reinforcement,  $\rho_y$  is transverse reinforcement ratio,  $f_c$  is concrete compressive strength,  $F_{yv}$  is yield strength of bars at vertical direction of wall,  $F_{yt}$  is strength of horizontal bars,  $N_u$  is applied load during experimental test, and  $V_u$  is shear strength capacity of the RCW.

**Table 5** Statistical properties of datasets for shear strength of RC wall

Variable	$X_{\min}$	$X_{\max}$	STD	Average
$l_w$ (mm)	450	3200	482.14	1423.32
$h_w$ (mm)	495	4928	1196.99	2544.06
$b_w$ (mm)	45	305	50.14	123.35
$A_g$ (mm <sup>2</sup> )	137,250	144,000	19,911.50	153,811.49
$h_w/l_w$	0.50	5.83	0.87	1.84
$\rho_x$	0	2.30	0.39	0.53
$\rho_y$	0	1.17	0.26	0.51
$f_c$ (MPa)	13.50	93.60	16.04	39.17
$F_{yv}$ (MPa)	289	414	146.16	487.66
$F_{yt}$ (MPa)	428.40	1187	162.65	506.17
$N_u$ (kN)	0	3312	634.01	720.75
$V_u$ (kN)	79.88	2532	588.59	627.85

### 5.1 Comparative metrics

Some statistical indices, such as root mean square error (RMSE), mean absolute error (MAE),  $R^2$ , Willmott index of agreement (WI), performance index (PI), and discrepancy ratio (DR), are employed and examined to assess predictive model adequacy in both training and testing phases:



$$R^2 = \frac{[\sum_{i=1}^n (o_i - \bar{o}) \times (p_i - \bar{p})]^2}{\sum_{i=1}^n (o_i - \bar{o})^2 \times \sum_{i=1}^n (p_i - \bar{p})^2} \tag{17}$$

$$RMSE = \sqrt{\frac{\sum_{i=1}^n (o_i - p_i)^2}{N}} \tag{18}$$

$$MAE = \frac{1}{n} \sum_{i=1}^n |o_i - p_i| \tag{19}$$

$$WI = 1 - \frac{\sum_{i=1}^n |(o_i - p_i)|^2}{\sum_{i=1}^n [|(o_i - \bar{o})| + |(p_i - \bar{p})|]^2}, \quad 0 < WI \leq 1 \tag{20}$$

$$PI_A = \frac{1}{4} \times \left( \frac{R_{min}^2}{R_A^2} + \frac{WI_{min}}{WI_A} + \frac{RMSE_A}{RMSE_{max}} + \frac{MAE_A}{MAE_{max}} \right) \tag{21}$$

$$DR_i = (p_i / o_i) - 1 \tag{22}$$

where  $o_i$  and  $p_i$  show observational and predicted values of the model, respectively, and  $\bar{o}$  and  $\bar{p}$  show mean observational and predicted values of the model,  $A$  and  $n$  denote the model under review and the total number of data, respectively.

MAE is an index of the difference in uncertainty among two measurements reflecting the identical phenomena (Willmott and Matsuura 2005). Variations of anticipated against reported and one analysing method versus another evaluation method are examples of  $o_i$  versus  $p_i$ .

WI or index of agreement was proposed by Willmott (Willmott 1981) as a predefined indicator of model projection uncertainty that ranges from 0 to 1. The WI is the proportion of mean square error to prospective error. A score of 1 shows a flawless coincidence, whereas a value of 0 implies no compatibility of any kind.

DR distinguishes the disparity between the reported and modelled amount of instances to the difference between the anticipated population and the estimation interval's limit.

With lower values for MAE, RMSE, and PI, higher values for  $R^2$ , and WI, the greatest accuracy can be obtained. Among other indices, DR shows information about error distribution. The predicted and observed values are equal when  $DR = 0$ , the predicted values are underestimated when  $DR < 0$ , and the predicted values are overestimated when  $DR > 0$ .

## 6 Results and discussion

For impactful model assessment and a preliminary examination of prediction accuracy, graphical techniques and quantitative indicators are essential. The scattered plot is a common graphical approach for assessing data distribution and variation.

The scatterplots for the training and testing datasets for anticipated and experimentally observed  $V_u$  are shown in

Fig. 5. For the projected data of all models, the perfect equity line of  $P = O$ , as well as the lines with +20% and -20% errors, are displayed.

According to the results shown in Fig. 5, the number of errors with predicted data in the more than +20% and less than -20% range for ANFIS is 71 (48 data in training and 23 data in testing), 44 for PSOFIS (27 data in training and 17 data in testing), 39 for GAFIS (24 data in training and 15 data in testing), and 37 data points (34 data in training and 15 data in testing) by using RF model.

Table 6 displays the performance of all examined models based on the RMSE,  $R^2$ , MAE, and WI criteria, providing for a more detailed comparison of the approaches. The index values for the RF, PSOFIS, and GAFIS models are near to each other in the training set. PSOFIS is ranked top based on  $R^2$ , RMSE, and MAE values, with RF, GAFIS, and ANFIS ranking in next places, respectively.

Based on  $R^2$  and RMSE in the testing phase, the RF with the greatest  $R^2$  and lowest RMSE (RMSE = 151.89 and  $R^2 = 0.9351$ ) is superior for testing data. PSOFIS is ranked second with (RMSE = 186.20 and  $R^2 = 0.891$ ), and GAFIS and ANFIS are ranked third and fourth, respectively, with (RMSE = 188.498 and  $R^2 = 0.889$ ) and (RMSE = 225.7 and  $R^2 = 0.84$ ). Based on MAE, RF is preferable with an MAE of 111.52, followed by GAFIS, PSOFIS, and ANFIS with MAEs of 114.39, 116.62, and 157.83, respectively.

A multi-index parameter (PI) is also utilized to measure the performance of the models. The index incorporates statistical indicators such as  $R^2$ , RMSE, MAE, and WI. According to equation 1, PI is between 0 and 1, with PI closer to 0 indicating the highest model accuracy. For test data, the performance index for RF is 0.81, putting it in the first place. PSOFIS and GAFIS, both with  $PI = 0.87$ , are ranked second, while ANFIS, with  $PI = 1$ , is ranked last.

Figure 6 depicts a comparison of frequency cumulative error (FCE) versus absolute relative error for the RF, PSOFIS, GAFIS, and ANFIS models in test and train data. It is possible to calculate the percentage of data that is less or more than the required number. For example, RF and hybrid techniques (PSOFIS and GAFIS) predicted 50% of data with less than 10% error in train data and 75% of data with less than 30% error in test data. In the test phase, PSOFIS predicted 7% for data with more than 60% inaccuracy, whereas GAFIS, RF, and ANFIS predicted 10, 15, and 22%, respectively.

The RMSE/d coefficient captures low-error based on the RMSE statistic and high-tendency based on the WI index for the optimal model performance. Thus, the model with the lowest RMSE/WI has the best predictive performance of all the models. Figure 7 shows the values of RMSE/WI ratios for the examined models, which include the RF, PSOFIS, GAFIS, and ANFIS. It can be observed that the suggested RF model has the lowest RMSE/WI value, while hybrid approaches are ranked second, and ANFIS is the third place.

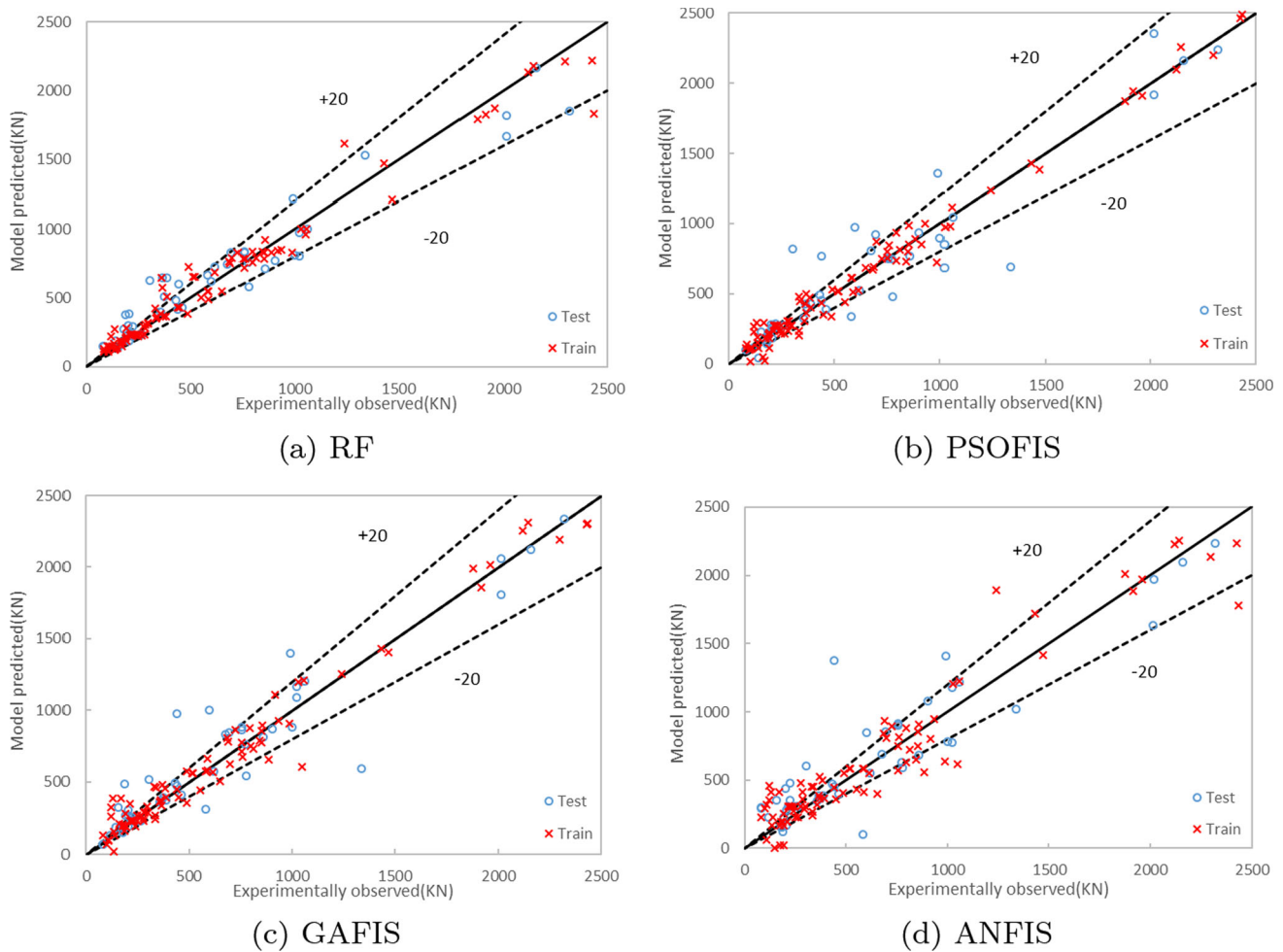


**Fig. 5** Measured and predicted value of  $V_u$  dimensions for test data

**Table 6** Statistical metrics in the train and test phase

Dataset	Method	$R^2$	RMSE	MAE	WI
Train	RF	0.9684	113.88	67.65	0.994
	PSOFIS	0.9823	80.19	60.33	0.995
	GAFIS	0.9665	110.72	79.06	0.997
	ANFIS	0.9150	175.03	69.70	0.987
Test	RF	0.9351	151.90	111.53	0.978
	PSOFIS	0.8909	186.21	116.63	0.970
	GAFIS	0.8895	188.50	114.39	0.971
	ANFIS	0.8409	225.27	157.83	0.956

Taylor diagram, which is composed of three statistical variables, including root, mean squared error, index of determination, and standard deviation, depicts the performance of the methods utilized in one basic illustration (Fig. 8).

The RF, PSOFIS, GAFIS, and ANFIS models may be rated from best to worst accuracy predictions based on the test

phase findings of the Taylor diagram. PSOFIS, RF, GAFIS, and ANFIS were rated best to worst during the train phase.

The effect of altering  $b_w$  and  $\rho_x$  on the proposed models' conclusions was investigated. The discrepancy ratio (DR), defined as the ratio of predicted and actual values, was used to determine the sensitivity of the proposed model to the  $b_w$  and  $\rho_x$  parameters. A DR of one implies complete cooperation, whereas numbers greater (or less than zero) indicate over- (or under-) prediction of the value of  $V_u$ . This is significant if the errors are negative; it indicates that the model forecasts the data value less than the true value, which has a negative performance, and large positive mistakes may raise the project's cost.

Figures 9 and 10 illustrate changes in DR values plotted against  $b_w$  and  $\rho_x$  for all models during the train and test phases. Among the models, the RF's DR errors are within a tolerable range ( $-0.25$  to  $1$ ). PSOFIS, GAFIS and ANFIS ranges are ( $-1.5$  to  $1.5$ ), ( $-2.5$  to  $2.2$ ), and ( $-2$  to  $2.5$ ), respectively. As a result, these three models frequently under-predict and over-predict the value of  $V_u$ .

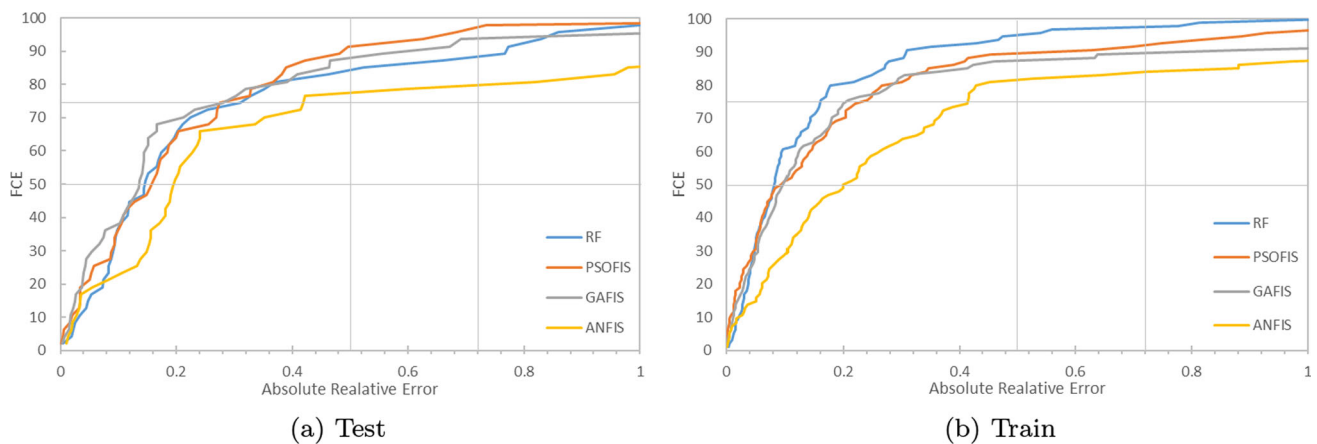


Fig. 6 The cumulative frequency against the absolute relative error for the models

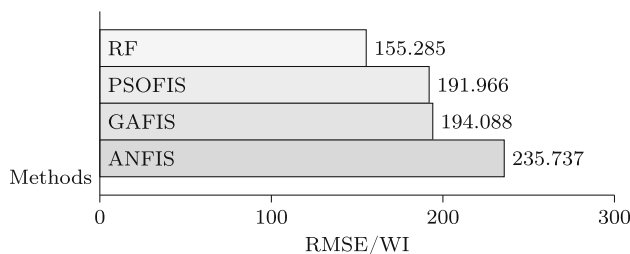


Fig. 7 RMSE/WI ratio for different models in testing phases

For  $b_w$  parameter, PSOFIS, GAFIS, and ANFIS model for  $40 < b_w < 100$  exhibited over-prediction and under-prediction, while DR values for  $100 < b_w < 300$  are close to zero that demonstrates a good match between the observed and anticipated  $V_u$ .

For  $\rho_x$  parameter, ANFIS model for all range of  $\rho_x$  and hybrid models for  $0 < \rho_x < 1$ , both have over-prediction and under-prediction. The RF model has consistent behaviour across all  $b_w$  and  $\rho_x$  ranges. RF outperforms the other models considered in this study in terms of DR.

### 6.1 Sensitivity analysis

Sensitivity analysis based on variable importance was conducted to decide the most effective parameters in the prediction of shear strength by the RF model. The significance of each variable is determined by examining the increase of prediction error when the OOB data for that variable is randomly permuted while all other variables remain constant (Goudarzi et al. 2014).

After setting the pre-selected optimal values of  $n_{tree}$  and  $m_{try}$  to decrease the uncertainty, 100 distinct forests were built, and the mean of significance was determined.

The sensitivity analysis for the variable’s relevance is shown in Fig. 11. It can be depicted that the wall thickness ( $b_w$ ) and concrete compressive strength ( $f_c$ ) have the

greatest and least influence on shear strength, respectively. Rebars strength at the vertical direction ( $F_{yv}$ ), the length of the wall ( $l_w$ ), and the gross area of the wall ( $A_g$ ) all have quite the same importance (around 8%). The next rank of varying importance is the height-to-length ratio ( $h_w/l_w$ ), length of the vertical steel reinforcement, ( $Tran.web$ ), rebars strength at the lateral direction ( $F_{ytTrans.}$ ) and  $N_u$ . Finally, the height of the wall ( $h_w$ ) and the compressive strength of the concrete ( $f_c$ ) have the least impact on shear strength.

## 7 Discussion and future research perspectives

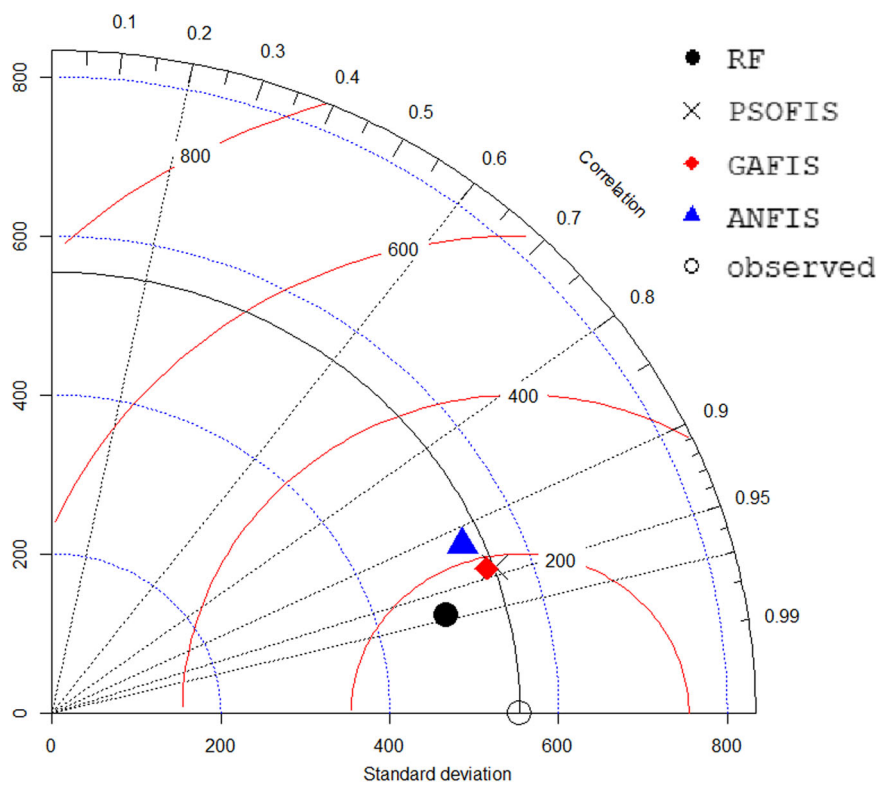
The results provided therein provide substantial insight into the performance and prediction capacities of several models used to estimate the shear strength of reinforced concrete walls. This section’s goal is to thoroughly examine and compare the results of the RF, PSOFIS, GAFIS, and ANFIS models, as well as to investigate the sensitivity of the suggested models to the parameters  $b_w$  and  $\rho_x$ .

Scatter plots were used to evaluate data distribution and variation to calculate prediction accuracy. The results indicate that all models forecast shear strength with varying degrees of accuracy. The perfect equity line (P=O) and lines representing +20% and -20% errors are provided for reference.

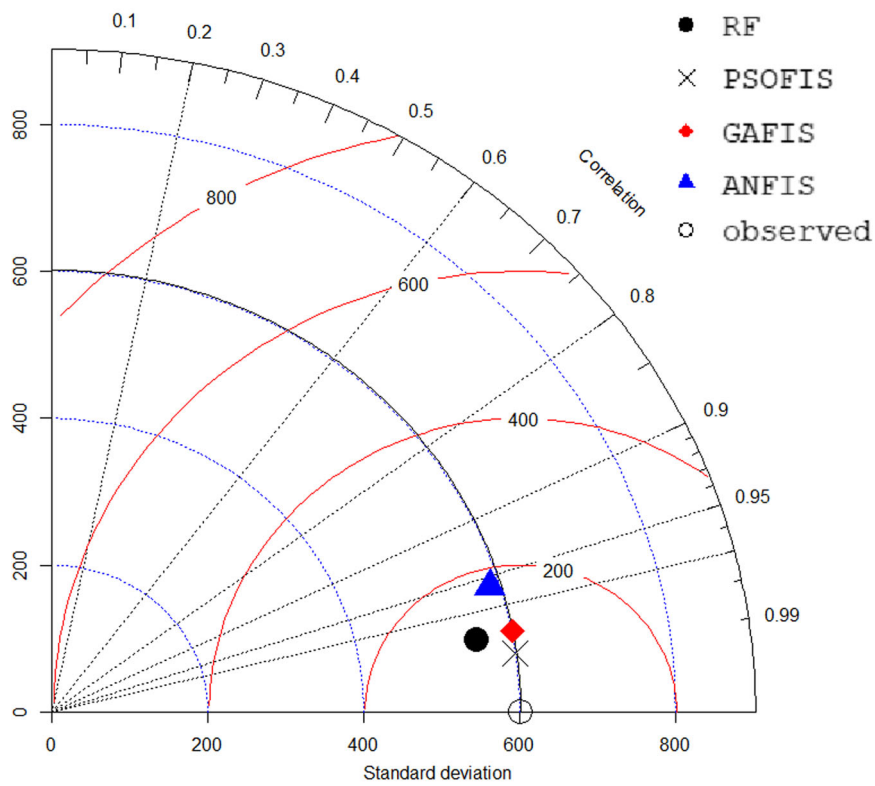
In the training set, RF, PSOFIS, GAFIS, and ANFIS all perform well, with PSOFIS having the greatest  $R^2$ , RMSE, and MAE values. RF, on the other hand, emerges as the superior model in the testing phase, with the greatest  $R^2$  (0.9351) and the lowest RMSE (151.90), as well as the lowest MAE (111.53). GAFIS and ANFIS are ranked second and third in terms of total prediction accuracy, respectively.

Additionally, the FCE study sheds light on the models’ ability to anticipate various degrees of error properly. RF

**Fig. 8** Taylor diagram for different models in the train and test phase



(a) Test



(b) Train

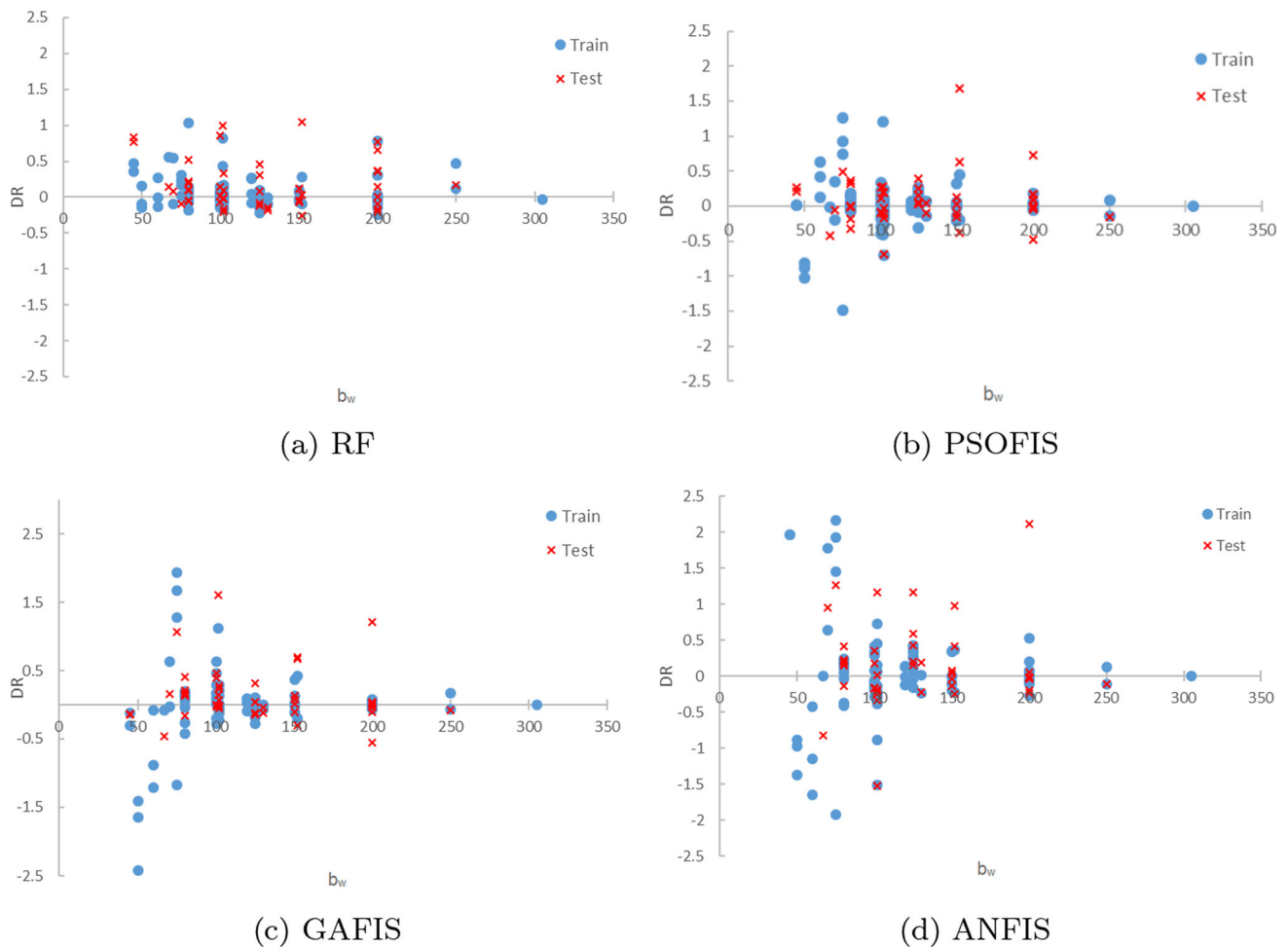


Fig. 9 DR values of  $b_w$  for different models in test and train data

and hybrid approaches (PSOFIS and GAFIS) outperform in the testing phase, successfully predicting a considerable percentage of data with less than 10 and 30% inaccuracy, respectively. ANFIS, on the other hand, reveals higher percentages of data with larger errors.

Based on the RMSE/WI ratios, in terms of overall accuracy, hybrid techniques (PSOFIS and GAFIS) rank second, while ANFIS trails behind.

The Taylor diagram, which combines numerous statistical variables, gives a succinct picture of the models' performance. Based on the test phase results, the accuracy forecasts of RF, PSOFIS, GAFIS, and ANFIS may be ordered from best to worst, with PSOFIS and RF beating the other models during the training phase.

The suggested models' sensitivity to the parameters  $b_w$  and  $\rho_x$  is also investigated. The discrepancy ratio (DR) is used to assess how well the models respond to changes in these parameters. The range of DR values for RF is consistently smaller (-0.25 to 1), indicating more dependable predictions. PSOFIS, GAFIS, and ANFIS have wider ranges,

indicating a tendency to both underestimate and overestimate shear strength values.

Regarding the parameter  $b_w$ , it is observed that PSOFIS, GAFIS, and ANFIS models exhibit over-prediction and under-prediction for  $40 < b_w < 100$ , while DR values tend to approach zero for  $100 < b_w < 300$ , indicating a better match between observed and predicted shear strengths.

ANFIS reliably over-predicts and under-predicts the parameter  $\rho_x$  over the full range, whereas hybrid models exhibit comparable performance for  $0 < \rho_x < 1$ . In contrast, the RF model consistently outperforms the other models in terms of DR throughout all  $b_w$  and  $\rho_x$  ranges.

The current study on determining the shear strength of reinforced concrete walls lays a solid platform for future research in this area. The data and technique given in this paper suggest various future research areas. We may provide light on the relevance of this study and its implications for future improvements.

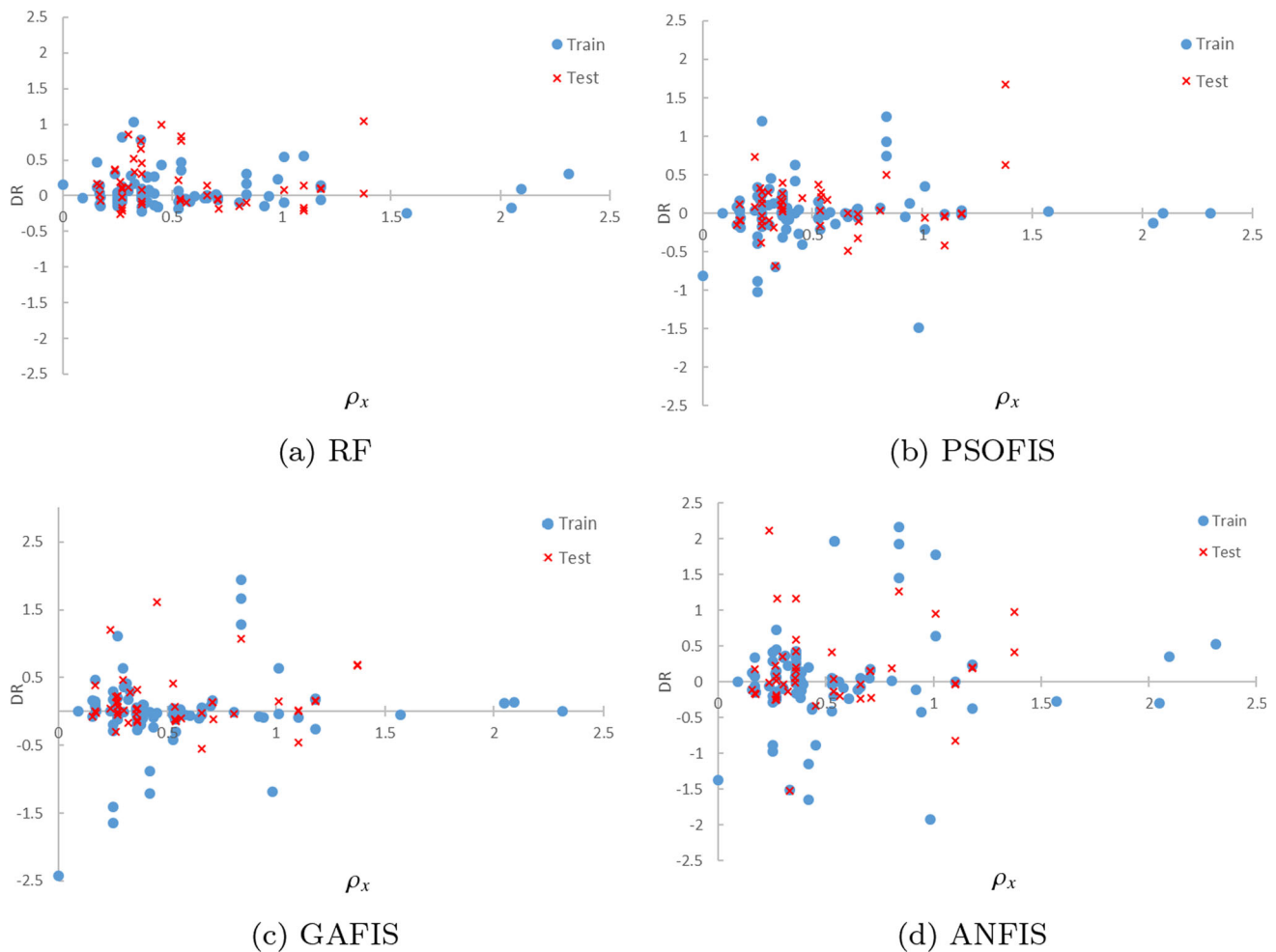


**Fig. 10** DR values of  $\rho_x$  for different models in test and train data

- Incorporation of additional input features: To estimate shear strength, the current study relied largely on a set of input features. Additional significant elements, such as concrete mix design parameters, reinforcing details, curing conditions, and environmental influences, should be investigated in future studies. By adding these elements, the prediction capacities of the models may be improved, resulting in more accurate shear strength calculations.
- Expansion to other types of concrete elements: This study concentrated on reinforced concrete walls. The created models, however, may be applied to different types of concrete parts such as beams, columns, slabs, and joints. Investigating the models' applicability to these elements would help to a more thorough knowledge of shear strength prediction in diverse structural components.
- Experimental data inclusion: The current investigation relied on both predicted and experimentally observed shear strength data. However, future studies may concentrate on gathering more experimental data from a broader range of test specimens. Integrating such experimental

- data into models can improve their dependability and generalizability.
- The current study focused on reinforced concrete walls with precise material attributes and mixed proportions. Future research can look into how the established models can be used in diverse concrete materials, such as high-strength concrete, self-compacting concrete, and fibre-reinforced concrete. This would provide a more comprehensive knowledge of shear strength prediction across different concrete compositions.
- Validation on real-life structures: To verify their practical feasibility, the created models may be validated on real-life reinforced concrete structures. Comparing projected shear strength values to actual measurements from existing structures would give useful information into the accuracy of the models and potential areas for improvement.
- Design guidelines development: Accurate calculation of shear strength in reinforced concrete buildings is critical for design and assessment. Future research might focus

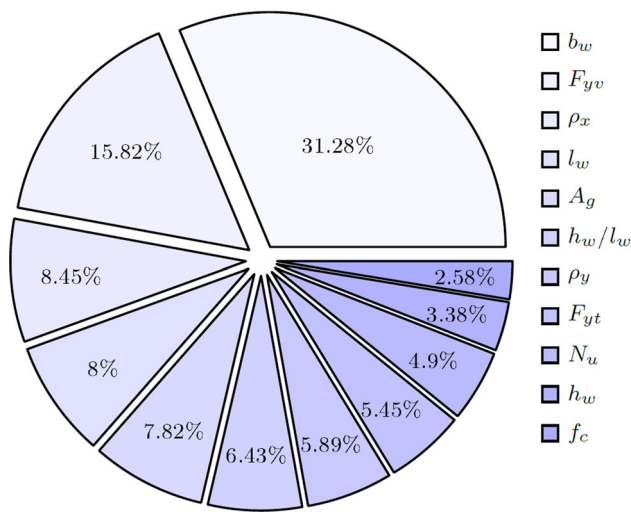


Fig. 11 Sensitivity analysis of parameters

on providing design guidelines or suggestions for professionals and engineers based on the findings of this study. These recommendations would make it more straightforward to choose appropriate models and give insights into the aspects that influence shear strength in reinforced concrete components.

### 8 Conclusions

While RCWs proved their feasibility as a most effective lateral resisting system for disturbances such as wind and seismic loads in civil structures, due to their diverse structural configurations, different loading situations, and the complex nonlinear relations between the input variables and the structural response, predicting their shear capacity is rather complicated. In this paper, the authors deploy different soft computing-based modelling approaches (RF, ANFIS, PSOFIS, and GAFIS) for predicting the shear capacity of RCWs. Based on this work, the following conclusions can be drawn:

- Current design codes have substantial uncertainty and do not completely reflect the effect of major design factors on shear strength in a logical way. The increased model variability vs the main design variables computed findings in this study for these approaches explicitly state this.
- The parametric analysis and different analytical measurements show that the developed innovative hybrid model addressed the impacts of the main design factors as well as the highly nonlinear relationship between the input design requirements and the projected shear capacity adequately.

- The suggested models might be advanced further to give specifications with higher prediction reliability and resilience for this realistic albeit complicated design challenge, therefore improving design precision.
- When compared to other techniques, the RF with the highest  $R^2$  (0.9351), lowest RMSE (151.89), and the best PI (0.81) was more accurate. It is also possible to conclude that RF is superior since its DR values are nearly equivalent to zero. Additionally, in terms of RMSE/WI, RF has the lowest value, making it more accurate than other models.
- Sensitivity analysis reveals that the thickness of the wall ( $b_w$ ) is the most important element influencing shear strength.
- PSOFIS and GAFIS (hybrid models) are more competent than ANFIS with the conventional optimization algorithm of enhancing the MF of fuzzy inference systems.
- There is a need to investigate new metaheuristic optimization algorithms that may be better adjusted for integration with the FIS model.

**Author Contributions** All authors contributed to the study’s conception and design. GP performed data collection. YS performed the analysis and model’s developments. The first draft of the manuscript was written and edited by AT and the work was supervised by MH-N and all authors commented on previous versions of the manuscript. All authors read and approved the final manuscript.

**Funding** The authors declare that no funds, grants, or other support were received during the preparation of this manuscript.

**Data Availability** The datasets generated during and/or analysed during the current study are available from the corresponding author upon reasonable request.

### Declarations

**Conflict of interests** The authors declare that they have no conflict of interest.

**Open Access** This article is licensed under a Creative Commons Attribution 4.0 International License, which permits use, sharing, adaptation, distribution and reproduction in any medium or format, as long as you give appropriate credit to the original author(s) and the source, provide a link to the Creative Commons licence, and indicate if changes were made. The images or other third party material in this article are included in the article’s Creative Commons licence, unless indicated otherwise in a credit line to the material. If material is not included in the article’s Creative Commons licence and your intended use is not permitted by statutory regulation or exceeds the permitted use, you will need to obtain permission directly from the copyright holder. To view a copy of this licence, visit <http://creativecommons.org/licenses/by/4.0/>.

## References

- Al-Furjan M, Shan L, Shen X, Kolahchi R, Rajak DK (2022) Combination of FEM-DQM for nonlinear mechanics of porous GPL-reinforced sandwich nanoplates based on various theories. *Thin-Walled Struct* 178:109495. <https://doi.org/10.1016/j.tws.2022.109495>
- Al-Furjan M, Xu MX, Farrokhan A, Jafari GS, Shen X, Kolahchi R (2022) On wave propagation in piezoelectric-auxetic honeycomb-2D-FGM micro-sandwich beams based on modified couple stress and refined zigzag theories. *Waves Random Complex Media* 22:1–25. <https://doi.org/10.1080/17455030.2022.2030499>
- Al-Furjan M, Yin C, Shen X, Kolahchi R, Zarei MS, Hajmohammad M (2022) Energy absorption and vibration of smart auxetic FG porous curved conical panels resting on the frictional viscoelastic torsional substrate. *Mech Syst Signal Process* 178:109269. <https://doi.org/10.1016/j.ymsp.2022.109269>
- Al-Obaidi M, Li JP, Kara-Zaïtri C, Mujtaba I (2017) Optimisation of reverse osmosis based wastewater treatment system for the removal of chlorophenol using genetic algorithms. *Chem Eng J* 316:91–100. <https://doi.org/10.1016/j.cej.2016.12.096>
- American Concrete Institute (2014) Building code requirement for reinforced concrete (ACI 318–14). MI, USA, American Concrete Institute
- Ansari M, Othman F, El-Shafie A (2020) Optimized fuzzy inference system to enhance prediction accuracy for influent characteristics of a sewage treatment plant. *Sci Total Environ* 722:137878. <https://doi.org/10.1016/j.scitotenv.2020.137878>
- Armaghani DJ, Hatzigeorgiou GD, Karamani C, Skentou A, Zoumpoulaki I (2019) Asteris PG Soft computing-based techniques for concrete beams shear strength. *Proc Struct Integr* 17:924–933. <https://doi.org/10.1016/j.prostr.2019.08.123>
- Asgarpoor M, Gharavi A, Epackachi S (2021) Investigation of various concrete materials to simulate seismic response of RC structures. *Structures* 29:1322–1351. <https://doi.org/10.1016/j.istruc.2020.11.042>
- Baghi H, Baghi H, Siavashi S (2019) Novel empirical expression to predict shear strength of reinforced concrete walls based on particle swarm optimization. *ACI Struct J* 116(5):247–61
- Breiman L (2001) Random Forests. *Mach Learn* 45(1):5–32. <https://doi.org/10.1023/A:1010933404324>
- Chandra J, Chanthabouala K, Teng S (2018) Truss model for shear strength of structural concrete walls. *ACI Struct J*. <https://doi.org/10.14359/51701129>
- Chen MY (2013) A hybrid anfis model for business failure prediction utilizing particle swarm optimization and subtractive clustering. *Inf Sci* 220:180–195. <https://doi.org/10.1016/j.ins.2011.09.013>
- Code P (2005) Eurocode 8: Design of structures for earthquake resistance-part 1: general rules, seismic actions and rules for buildings. European Committee for Standardization, Brussels
- Committee ACI (1995) Building code requirements for structural concrete: (ACI 318–95); and commentary (ACI 318R–95). American Concrete Institute, USA
- Darwin D, Dolan CW, Nilson AH (2016) Design of concrete structures, vol 2. McGraw-Hill Education New York, USA
- Goldberg DE (2006) Genetic algorithms. Pearson Education India, Karnataka
- Gondia A, Ezzeldin M, El-Dakhkhni W (2020) Mechanics-guided genetic programming expression for shear-strength prediction of squat reinforced concrete walls with boundary elements. *J Struct Eng* 146(11):04020223. [https://doi.org/10.1061/\(ASCE\)ST.1943-541X.0002734](https://doi.org/10.1061/(ASCE)ST.1943-541X.0002734)
- Goudarzi N, Shahsavani D (2012) Application of a random forests (RF) method as a new approach for variable selection and modelling in a QSRR study to predict the relative retention time of some polybrominated diphenylethers (pbdes). *Anal Methods* 4:3733–3738. <https://doi.org/10.1039/C2AY25484K>
- Goudarzi N, Shahsavani D, Emadi-Gandaghi F, Chamjangali MA (2014) Application of random forests method to predict the retention indices of some polycyclic aromatic hydrocarbons. *J Chromatogr A* 1333:25–31. <https://doi.org/10.1016/j.chroma.2014.01.048>
- Gulec CK, Whittaker AS, Stojadinovic B (2007) Shear strength of squat reinforced concrete walls with flanges and barbell pp 1–8
- Hadzima-Nyarko M (2015) Comparison of fundamental periods of reinforced shear wall dominant building models with empirical expressions. *Tehnicky vjesnik-Technical Gazette* 22(3):685–694. <https://doi.org/10.17559/TV-20140228124615>
- Hadzima-Nyarko M, Ademović N, Krajnović M (2021) Architectural characteristics and determination of load-bearing capacity as a key indicator for a strengthening of the primary school buildings: Case study osijek. *Structures* 34:3996–4011. <https://doi.org/10.1016/j.istruc.2021.09.105>
- Holland JH et al (1992) Adaptation in natural and artificial systems: an introductory analysis with applications to biology, control, and artificial intelligence. MIT press, USA
- Jang JS (1993) Anfis: adaptive-network-based fuzzy inference system. *IEEE Trans Syst Man Cybern* 23(3):665–685. <https://doi.org/10.1109/21.256541>
- Kennedy J, Eberhart R (1995) Particle swarm optimization. In: Proceedings of ICNN'95 - international conference on neural networks, vol. 4, pp 1942–1948. <https://doi.org/10.1109/ICNN.1995.488968>
- Keshtegar B, Nehdi ML, Kolahchi R, Trung NT, Bagheri M (2021) Novel hybrid machine learning model for predicting shear strength of reinforced concrete shear walls. *Eng Comput*. <https://doi.org/10.1007/s00366-021-01302-0>
- Keshtegar B, Nehdi ML, Trung NT, Kolahchi R (2021) Predicting load capacity of shear walls using svr-rsm model. *Appl Soft Comput* 112:107739. <https://doi.org/10.1016/j.asoc.2021.107739>
- Keshtegar B, Bouchouicha K, Bailek N, Hassan MA, Kolahchi R, Despotovic M (2022) Solar irradiance short-term prediction under meteorological uncertainties: survey hybrid artificial intelligent basis music-inspired optimization models. *Eur Phys J Plus* 137(3):362. <https://doi.org/10.1140/epjp/s13360-022-02371-w>
- Kolahchi R, Keshtegar B, Trung NT (2022) Optimization of dynamic properties for laminated multiphase nanocomposite sandwich conical shell in thermal and magnetic conditions. *J Sandwich Struct Mater* 24(1):643–662. <https://doi.org/10.1177/10996362211020388>
- Koza J (1994) Genetic programming as a means for programming computers by natural selection. *Stat Comput* 4(2):87–112. <https://doi.org/10.1007/BF00175355>
- Kusunoki K, Sakashita M, Mukai T, Tasai A (2019) Study on the accuracy of practical functions for R/C wall by a developed database of experimental test results. *Bull Earthq Eng* 17(12):6621–6644. <https://doi.org/10.1007/s10518-019-00691-4>
- Luo C, Keshtegar B, Zhu SP, Niu X (2022) EMCS-SVR: hybrid efficient and accurate enhanced simulation approach coupled with adaptive SVR for structural reliability analysis. *Comput Methods Appl Mech Eng* 400:115499. <https://doi.org/10.1016/j.cma.2022.115499>
- Mangalathu S, Jang H, Hwang SH, Jeon JS (2020) Data-driven machine-learning-based seismic failure mode identification of reinforced concrete shear walls. *Eng Struct* 208:110331. <https://doi.org/10.1016/j.engstruct.2020.110331>
- Marzok A, Lavan O, Dancygier A (2020) Predictions of moment and deflection capacities of RC shear walls by different analytical models. *Structures* 26:105–127. <https://doi.org/10.1016/j.istruc.2020.03.059>
- Nguyen DD, Tran VL, Ha DH, Nguyen VQ, Lee TH (2021) A machine learning-based formulation for predicting shear capacity of squat



- flanged RC walls. *Structures* 29:1734–1747. <https://doi.org/10.1016/j.istruc.2020.12.054>
- Nikoo M, Hadzima-Nyarko M, Khademi F, Mohasseb S (2017) Estimation of fundamental period of reinforced concrete shear wall buildings using self organization feature map. *Struct Eng Mech* 63(2):237–249. <https://doi.org/10.12989/SEM.2017.63.2.237>
- Piri J, Abdollahipour M, Keshtegar B (2023) Advanced machine learning model for prediction of drought indices using hybrid SVR-RSM. *Water Resour Manage* 37(2):683–712. <https://doi.org/10.1007/s11269-022-03395-8>
- Rani D, Moreira MM (2010) Simulation-optimization modeling: a survey and potential application in reservoir systems operation. *Water Resour Manage* 24(6):1107–1138. <https://doi.org/10.1007/s11269-009-9488-0>
- Sharafati A, Tafarajnoruz A, Shourian M, Yaseen ZM (2020) Simulation of the depth scouring downstream sluice gate: the validation of newly developed data-intelligent models. *J Hydro-environ Res* 29:20–30. <https://doi.org/10.1016/j.jher.2019.11.002>
- Tabrizikahou A, Kuczma M, Łasecka-Plura M (2022) Out-of-plane behavior of masonry prisms retrofitted with shape memory alloy stripes: numerical and parametric analysis. *Sensors* 22(20):8004. <https://doi.org/10.3390/s22208004>
- Tabrizikahou A, Kuczma M, Łasecka-Plura M, Noroozinejad Farsangi E (2022) Cyclic behavior of masonry shear walls retrofitted with engineered cementitious composite and pseudoelastic shape memory alloy. *Sensors* 22(2):511. <https://doi.org/10.3390/s22020511>
- Takagi T, Sugeno M (1985) Fuzzy identification of systems and its applications to modeling and control. *IEEE Trans Syst, Man, Cybern SMC*–15(1):116–132
- Teng S, Chandra J (2016) Cyclic shear behavior of high strength concrete structural walls. *ACI Struct J* 113(6):1335–1345
- Willmott CJ (1981) On the validation of models. *Phys Geogr* 2(2):184–194. <https://doi.org/10.1080/02723646.1981.10642213>
- Willmott CJ, Matsuura K (2005) Advantages of the mean absolute error (MAE) over the root mean square error (RMSE) in assessing average model performance. *Climate Res* 30(1):79–82
- Wood Sharon L (1990) Shear strength of low-rise reinforced concrete walls. *ACI Struct J* 87(1):99–107
- Zhu SP, Keshtegar B, Ben Seghier MEA, Zio E, Taylan O (2022) Hybrid and enhanced PSO: Novel first order reliability method-based hybrid intelligent approaches. *Comput Methods Appl Mech Eng* 393:114730. <https://doi.org/10.1016/j.cma.2022.114730>

**Publisher's Note** Springer Nature remains neutral with regard to jurisdictional claims in published maps and institutional affiliations.